# Hydrothermal synthesis and thermal properties of a novel cubic $ZrW_{1.80}V_{0.20}O_{7.90}$ solid solution

Xi Chen [a,c], Xuebin Deng [a], Hui Ma [a], Juzhou Tao [b], Xinhua Zhao [a,*]

[a] College of Chemistry and Analysis and Test Center, Beijing Normal University, Beijing 100875, PR China
[b] Experimental Physics Center, Institute of High Energy Physics, Chinese Academy of Sciences, Beijing 100049, PR China
[c] School of Civil Engineering and Communication, North China University of Water Source and Electric Power, Zhengzhou 450011, PR China

## ABSTRACT

Tetragonal $ZrW_{1.80}V_{0.20}O_{6.90}(OH)_{2.00}(H_2O)_{2.00}$ hydrate was prepared using an acidic steam hydrothermal (ASH) method. Thermal dehydration followed by phase transformation of this precursor leads to successful synthesis of a novel W-site low-valent substituted cubic $ZrW_{1.80}V_{0.20}O_{7.90}$ solid solution, the mechanism of this process is studied in detail revealing the hydrate and a metastable orthorhombic phase of $V'_W$ substitution solid solution as important intermediate product. This material is found to possess thermal contraction and order–disorder phase transformation properties similar to that of the cubic $ZrW_2O_8$.

© 2011 Elsevier Inc. All rights reserved.

## 1. Introduction

Cubic $ZrW_2O_8$ ($c$-$ZrW_2O_8$) and related compounds have attracted considerable research attention in lattice dynamics physics, solid oxide chemistry and material fields for the last two decades due to their strong isotropic negative thermal expansion (NTE) at high temperature over a wide temperature range [1]. For material application of $c$-$ZrW_2O_8$-type solid, it is desirable to alter their order–disorder phase transition temperature [2], increase ionic conductivity [3], enhance their strength of compression [4] and improve thermal stability simultaneously [5]. The main approach toward such material optimization goals is by synthesizing and studying cation substituted $Zr_{1-x}M_xW_{2-y}M'_yO_{8-z}$ solid solution with $c$-$ZrW_2O_8$ type crystal structure. So far successful substitution of $c$-$ZrW_2O_8$ focuses on the Zr site [2,6–10] and the substitution of Mo (VI) ion [5,11] for W (VI).

$ZrV_2O_7$ is another important isotropic NTE material [12–14] with a structure closely related to that of $c$-$ZrW_2O_8$ and consisting of corner-sharing octahedron and tetrahedron. Employing chemical and structural similarities between $ZrW_2O_8$ and $ZrV_2O_7$, the first aliovalent substituted cubic solid solution $\beta$-$ZrW_{1.8}V_{0.2}O_{7.9}$ was successfully synthesized by a precursor transition method, and its refined structure of a disordered crystal reported recently [15].

Direct synthesis of $ZrW_{1.8}V_{0.2}O_{7.9}$ by solid state reaction has not been achieved so far simply because vanadium oxide

sublimes at the high temperature range, where $ZrW_2O_8$ forms. It is therefore of interest to study the reaction mechanism of this precursor route, through which $ZrW_{1.8}V_{0.2}O_{7.9}$ was successfully prepared.

In this work, dehydration and phase transformation mechanism of such an acidic steam hydrothermal–thermal dehydrating precursor process (ASH–TDP) for preparing aliovalent substituted cubic-$ZrW_{1.80}V_{0.20}O_{7.90}$ was investigated using XRD, TG–DSC–QMS and Raman spectroscopy methods. The properties of ordered $\alpha$-$ZrW_{1.80}V_{0.20}O_{7.90}$ solid solution were also studied.

## 2. Experimental section

### 2.1. Synthesis of hydrated precursor and cubic $ZrW_{2.00-x}V_xO_{8.00-x/2}$ ($x=0$, 0.20) solid solution

The hydrated tetragonal precursors (denoted as HT-precursors) as well as byproduct $NH_4Cl$ were first obtained through an ASH route at 473 K for 24 h as described in Refs. [15,16], using AR grade $ZrOCl_2 \cdot 8H_2O$, $(NH_4)_6W_7O_{24} \cdot 6H_2O$ and $NH_4VO_3$ as reactants. Residual solution after the ASH process was examined for dissolved metal contents by ICP–AES (inductively coupled plasma torch, JY, VITIMA, France) spectroscopy.

On heating HT-precursor to 873 and 813 K for 2 h, respectively, $NH_4Cl$ was decomposed and single phase $c$-$ZrW_{2.00}O_{8.00}$ and $ZrW_{1.80}V_{0.20}O_{7.90}$ were produced.

To avoid interference of $NH_4Cl$ in studying the HT-precursor thermal dehydration mechanism, pure HT-precursors

$ZrW_{2.00}O_{7.00}(OH)_{2.00} \cdot (H_2O)_{2.00}$ and $ZrW_{1.80}V_{0.20}O_{6.90}(OH)_{2.00} \cdot (H_2O)_{2.00}$ were prepared by re-hydration of cubic $ZrW_{2.00}O_{8.00}$ and $ZrW_{1.80}V_{0.20}O_{7.90}$ using 20 mL of 10 mol L$^{-1}$ as the acidic steam source three times. Unsaturated tetragonal hydrated $ZrW_{1.80}V_{0.20}O_{6.90}(OH)_{2.00}(H_2O)_{2.00-\delta}$ was prepared similarly using 8 mol L$^{-1}$ HNO$_3$ as the acidic steam source.

2.0000 g HT-precursors of samples were heated at 500 K until the weight remains constant for accurate weight loss measurements.

## 2.2. Measurement and characterization

All X-ray diffraction (XRD) patterns were collected on a Philips X'Pert MPD diffractometer with X'Celerator detector using Cu-K$\alpha$ radiation. The XRD data were collected from 10° to 120° ($2\theta$) at 0.0167° ($2\theta$) step size and 20 s step time. For phase identification XRD data were collected from 10° to 70° ($2\theta$) and 10 s step time, and the data were indexed using PowderX program [17]. The precise lattice parameters at room temperature were calculated from XRD data calibrated with a SiO$_2$ internal standard (JCPDS-PDF: 33-1161, Quartz) using the Unitcell software [18].

*In situ* variable temperature XRD experiments were performed between room temperature to 573 K under flowing nitrogen gas using an Anton Paar TCU 2000 Temperature Control Unit, with sample mounted in an Anton Paar HTK 16 High-Temperature Chamber. Before data collection at each temperature, 3 min interval was kept to make sample achieve thermal equilibrium. Temperature monitoring of all XRD measurements were calibrated by KCl [19] as internal standard.

Quantitative Phase Analysis of polycrystalline materials using X-ray powder diffraction combining Rietveld and Reference Intensity Ratio (Rietveld-RIR QPA) analyses was performed to detect amount of amorphous phase in the ASH products. 0.20 g KCl as an internal standard was added to 2.02 g products. The crystalline phase fractions of the mixture were refined using GSAS software [20]. The crystal structure models used in Rietveld-RIR QPA refer to Ref. [19,21] for KCl and $ZrW_{2-x}V_xO_{7-x/2}(OH)_{2.00} \cdot (H_2O)_{2.00}$, respectively.

Linear dimension change of ceramic pellet with temperature was measured along the pellet diametrical direction by thermal mechanical analysis (TMA Q400, TA-Instruments). The data were collected at a heating rate of 3 K/min from room temperature to 523 K under a constant force of 0.1 N. The peak temperature of TMA curve was calibrated with Al cylinder standard and accurate to $\pm 1$ K. The TMA data were analyzed by the TA Universal Analysis software [22].

Differential Scanning Calorimetry–Thermal Gravimetric Analysis–Quadruple Mass Spectrometry (DSC–TGA–QMS) measurement was performed at a heating rate of 30 K/min using STA 449C/QMS 403C (Netzsch) under nitrogen gas flow.

Quantitative IR-spectra were measured on a Nicolet Avatar 360 FTIR Spectrometer (400–4000 cm$^{-1}$, 4 cm$^{-1}$ resolution, 128 scans) using the KBr pellet technique. 6.00 mg sample and 200.00 mg KBr were mixed and pressed into sample—KBr pellet. All pellets were dried at 313 K for 30 min under IR lamp to reduce the amount of absorbed water in crystal below 2 wt%.

Raman spectra were recorded with a Renishaw inVia Plus spectrometer in the 100–4000 cm$^{-1}$ range with a scan time 10 s. The 514.5 nm line of an Argon ion laser was used as the excitation source. Powder sample data in variable temperature were collected at 293, 303, 323, 353, 373, 393, 423, 443, 473, 493, 513, 533, 553 and 573 K at a heating rate of 30 K/min and a thermal equilibrium interval of 5 min.

## 3. Results and discussions

### 3.1. Characterization of the HT-precursors

The ICP–AES measurements indicate that relative amount of Zr, W, V elements dissolved in residual solution after the ASH process is less than 0.1 mol%, confirming no significant loss of metals in the ASH process. XRD patterns of the HT-precursors were indexed consistently to that of tetragonal $ZrMo_2O_7(OH)_2 \cdot (H_2O)_2$ (S.G: $I4_1cd$) as shown in Fig. 1. The lattice parameters are $a=11.4375(1)$ Å, $c=12.4950(2)$ Å and $a=11.4371(2)$ Å, $c=12.4810(5)$ Å for precursors of c-ZrW$_2$O$_8$ and ZrW$_{1.8}$V$_{0.2}$O$_{7.9}$, respectively, which is close to $a=11.45$ Å, $c=12.49$ Å of $ZrMo_2O_7(OH)_2 \cdot (H_2O)_2$ [21].

The amounts of amorphous phase is converge to 0.2(3)% and 0.1(2)% for the samples of $ZrW_{2.00-x}V_xO_{7.00-x/2}(OH)_{2.00}(H_2O)_{2.00}$ ($x=0$, 0.20) in the Rietveld-RIR QPA refinements, respectively. Gualtieri et al. indicated that the accuracy of amorphous phase in the sample was determined with absolute error close to 1 wt% when 10 wt% standard is added by using the Rietveld-RIR QPA method [23]. It is rational to believe that the actual amounts of amorphous phase are less than about 1 wt% although the refined results may be underestimation of the amorphous fraction. These results confirm HT-precursors are crystallite products with the targeted compositions. The details of Rietveld-RIR QPA refinement are shown in Appendix A (Supporting Information I).

Accurate measurements of weight loss after heating HT-precursors above their dehydration temperatures until constant weight are $8.40 \pm 0.03$ wt% (theoretical: 8.43%) and $8.80 \pm 0.02$ wt% (8.81%) for $ZrW_{2.00-y}V_yO_{7.00-y/2}(OH)_{2.00}(H_2O)_{2.00}$ ($y=0$ and 0.20), respectively. The weight loss of dehydration process corresponds to the following Eq. (1):

$$ZrW_{2.00-y}V_yO_{7.00-y/2}(OH)_{2.00}(H_2O)_{2.00}$$
$$= ZrW_{2.00-y}V_yO_{8.00-y/2} + 3.00H_2O \quad (y=0, 0.20) \qquad (1)$$
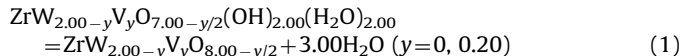
$ZrW_2O_7(OH)_2(H_2O)_2$ is a heterogeneous isomorphism of $ZrMo_2O_7(OH)_2(H_2O)_2$ [24] and has similar atomic coordination. Its structure resembles that of $ZrMo_2O_7(OH)_2(H_2O)_2$ and is a three-dimensional rigid network composed of [ZrO$_3$(OH)$_2$O$_2$]-pentagonal bi-pyramid and distorted [WO$_4$(OH)(H$_2$O)] octahedron chains cross-linked through oxygen atoms [21]. In order to reveal the configuration of V substitution in structure, Raman spectra of both $ZrW_{1.80}V_{0.20}O_{6.90}(OH)_{2.00}(H_2O)_{2.00}$ and $ZrW_2O_7(OH)_2(H_2O)_2$ were measured and compared as shown in Fig. 2. Based on an empirical relationship established by Hardcastle and Wachs [25] relevant
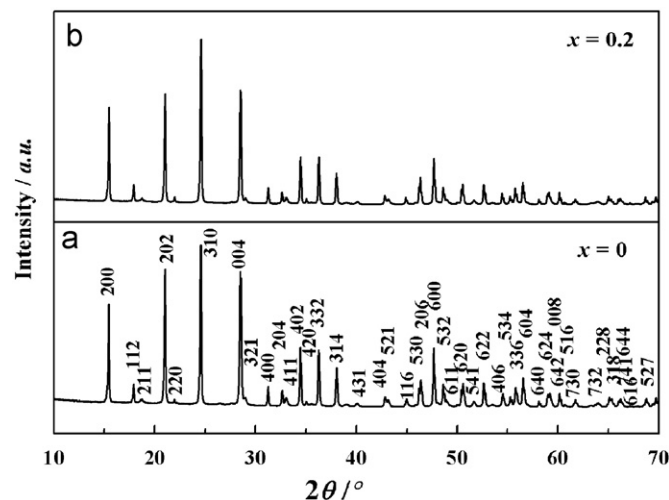


**Fig. 1.** Indexed XRD patterns of $ZrW_{2.00-y}V_yO_{7.00-y/2}(OH)_{2.00}(H_2O)_{2.00}$ ($y=0$, 0.20).
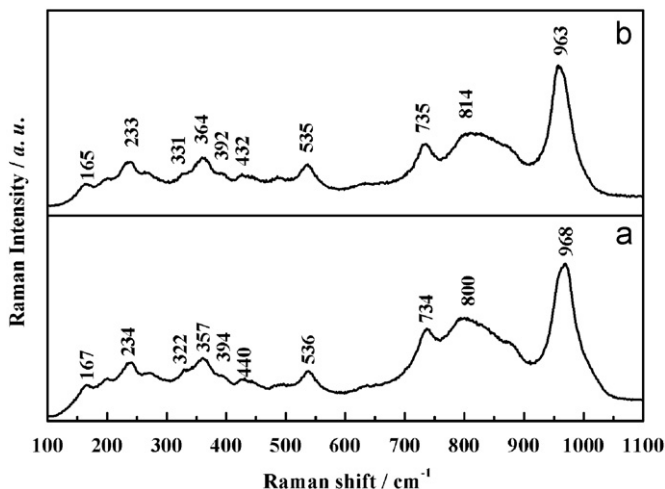
**Fig. 2.** Raman spectra of $ZrW_{2.00}O_{7.00}(OH)_{2.00}(H_2O)_{2.00}$ (a) and $ZrW_{1.80}V_{0.20}O_{6.90}$ $(OH)_{2.00}(H_2O)_{2.00}$ (b) at room temperature.

**Table 1**
Raman frequency for stretching vibration of [W/V]$O_6$ octahedron in $ZrW_{2-y}$ $V_yO_{7-y/2}(OH)_{2.00}(H_2O)_{2.00}$ (y=0, 0.20).

| $WO_6$ | [W/V]$O_6$ | $\tilde{\nu}$ (cm$^{-1}$)[a] | $s$ (vu)[b] | $R$ (Å)[c] | Assignment |
|---|---|---|---|---|---|
| 968 | 963 | 976 | 1.827 | 1.722 | W=O3 |
|  |  | 917 | 1.630 | 1.755 | W–O6 |
| 800 | 814 | 847 | 1.415 | 1.797 | W–O5 |
| 536 | 535 | 539 | 0.673 | 2.034 | W–O8 |
| 440 | 432 | 464 | 0.535 | 2.113 | W–O7 |
| 322 | 331 | 319 | 0.313 | 2.310 | W–O4 |

The Raman shift ($\nu\sim$) and bond valence ($s$) are derived from:

[a] $\tilde{\nu}/cm^{-1} = 25823\exp(-1.902R)$ [25];
[b] $s(W–O)/valence\ unit = (R/1.904)^{-6.0}$ [25];
[c] The diatomic distances ($R$) refer to Ref. [21].

**Table 2**
Bending/external Raman vibrational frequency (in cm$^{-1}$) of $ZrW_{2-y}V_yO_{7-y/2}$ $(OH)_{2.00}(H_2O)_{2.00}$ (y=0, 0.20) [26,27].

| Assignment[a] | y=0 | y=0.20 | Ref. value |
|---|---|---|---|
| $\nu_{as}$ (M–O) | 734 | 735 | 753 [26] |
| $\delta_s$ ($MO_6$) | 394 | 392 | 346–409 [26] |
| $\delta_s$ ($MO_6$) | 357 | 364 | 330 [27] |
| $\delta_s$ ($MO_6$) | 234 | 233 | 239 [26] |
| External mode | 167 | 165 | 178 [26] |

[a] M represents W atom in $ZrW_{2.00}O_{7.00}(OH)_{2.00}(H_2O)_{2.00}$ and W/V statistical atom in $ZrW_{1.80}V_{0.20}O_{6.90}(OH)_{2.00}(H_2O)_{2.00}$.

Raman stretching mode frequencies were estimated based on bond lengths in the distorted $WO_6$ polyhedron in $ZrW_{2.00}O_{7.00}$ $(OH)_{2.00}(H_2O)_{2.00}$ [21,24] and assigned to the measured Raman spectrum as listed in Table 1.

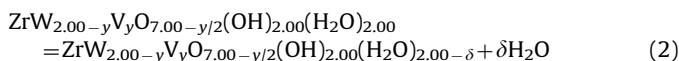The assigned stretching vibration frequencies of $MO_6$ octahedron in $ZrW_{2-y}V_yO_{7-y/2}(OH)_{2.00}(H_2O)_{2.00}$ are listed in Table 1. The other Raman spectrum peaks in Fig. 2(a) are identified as bending/external vibrational modes and listed in Table 2.

Fig. 2 compares the Raman spectra of $ZrW_{2.00-y}V_yO_{7.00-y/2}$-$(OH)_{2.00}(H_2O)_{2.00}$ solid solution with those of pure W hydrate. No significant feature changes were observed, and frequency shifts of $MO_6$ octahedral ($\nu_s$, $\nu_{as}$, $\delta_{as}$) stretching modes are especially small. Such evidence strongly supports that $V^{5+}$ ions only substitute for $W^{6+}$ sites and the original configuration of [W/V]$O_6$ polyhedral cross-linking with $ZrO_7$ polyhedral is maintained in the structure of $ZrW_{1.80}V_{0.20}O_{6.90}(OH)_{2.00}(H_2O)_{2.00}$.

## 3.2. Dehydration and phase transformation of $ZrW_{2-y}V_yO_{7-y/2}$ $(OH)_2(H_2O)_2$

The QMS and weight loss curves of saturated hydrate $ZrW_{2.00}O_{7.00}(OH)_{2.00}(H_2O)_{2.00}$ through TG measurement are plotted in Fig. 3(a) and those of unsaturated $ZrW_{1.80}V_{0.20}O_{6.90}$-$(OH)_{2.00}(H_2O)_{1.79}$ in Fig. 3(b). It is clear that the tetragonal phases undergo a dehydration process and the dehydration involves multiple steps. The DSC data in Fig. 3 indicate a slow endothermic processes starting at 363 and 369 K for $ZrW_{2.00}O_{7.00}(OH)_{2.00}$ $(H_2O)_{2.00}$ and $ZrW_{1.80}V_{0.20}O_{6.90}(OH)_{2.00}(H_2O)_{1.79}$ with 1.3 wt% and 0.9 wt% respective water loss according to the TG curves. At 460 and 440 K, discontinuous changes appear in the DTG curves revealing the occurrence of a separate process. From these temperatures up to about 510 K, dehydration rate accelerates to reach its maximum.

With the assumption that only crystalline water is removed (hydroxo-(O–H) group in the hydrate retained) below 450 K, the first stage of reaction is expressed as:

$$ZrW_{2.00-y}V_yO_{7.00-y/2}(OH)_{2.00}(H_2O)_{2.00}$$
$$=ZrW_{2.00-y}V_yO_{7.00-y/2}(OH)_{2.00}(H_2O)_{2.00-\delta}+\delta H_2O \qquad (2)$$

where $\delta$ is a measure of the degree of dehydration obtained through weight loss calculation and solely determines chemical composition of partially dehydrated hydrate.

As expected for the IR spectra a linear relationship consistent with the Eq. (2) exists between the absorbance ratio ($A_{H_2O}/A_{OH}$) and relative concentration ($C_{H_2O}/C_{OH}$) in saturated hydrate $ZrW_{2.00-y}V_yO_{7.00-y/2}(OH)_{2.00}(H_2O)_{2.00}$ (y=0, 0.20). This dependency at different degrees of dehydration is displayed in Fig. 4.
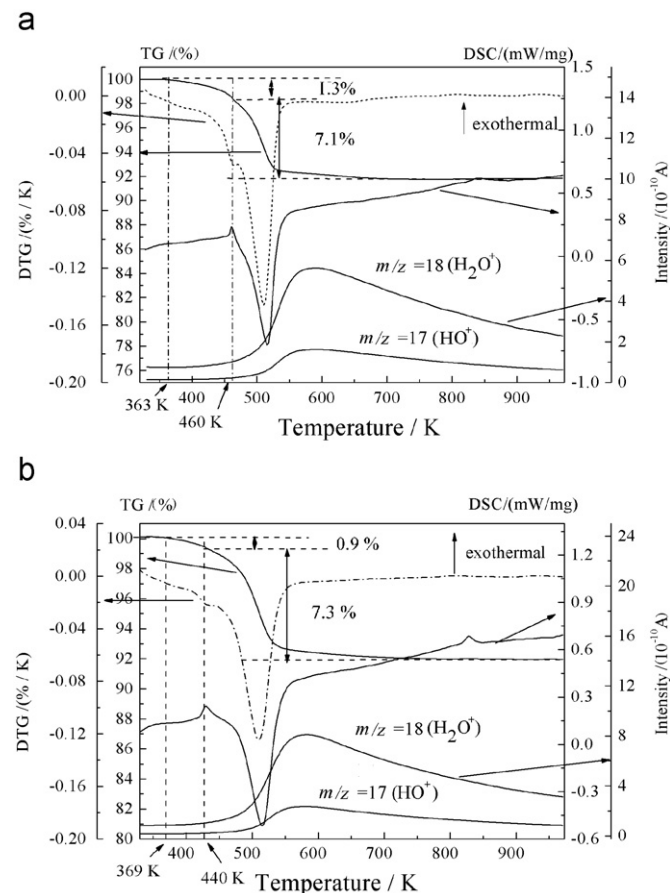


**Fig. 3.** TG–DSC–QMS curves of (a) $ZrW_{2.00}O_{7.00}(OH)_{2.00}(H_2O)_{2.00}$; (b) $ZrW_{1.80}V_{0.20}$-$O_{6.90}(OH)_{2.00}(H_2O)_{1.79}$.
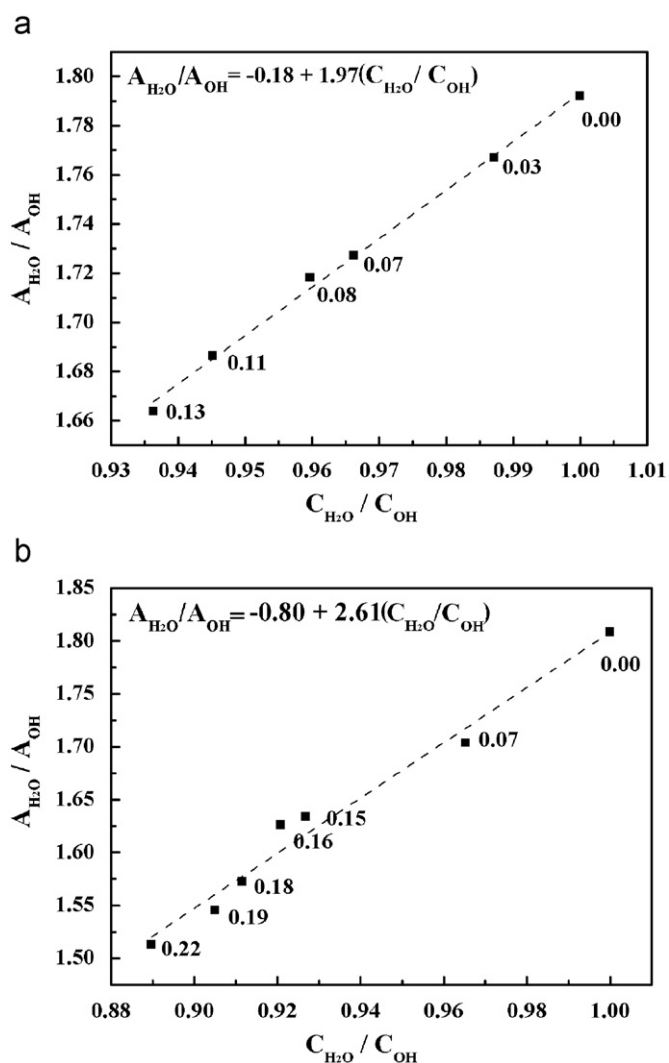
a



b



**Fig. 4.** IR absorbance ratio ($A_{H_2O}/A_{OH}$) of aquo-(O–H) to hydroxo-(O–H) groups (wave numbers 2980 and 3180 cm$^{-1}$ respectively) changes with their relative concentration ($C_{H_2O}/C_{OH}$) in ZrW$_{2.00-y}$V$_y$O$_{7.00-y/2}$(OH)$_{2.00}$(H$_2$O)$_{2.00}$ below 453 K. (a : $y$=0; b: $y$=0.20; $\delta$ values in Eq. (2) are labeled by the data points).

Fig. 5 shows the variable temperature XRD patterns of ZrW$_{2.00-y}$O$_{7.00-y/2}$(OH)$_{2.00}$(H$_2$O)$_{2.00-\delta}$ ($y$=0, 0.20). It was found that the tetragonal structure was stable up to approximate 453 K. Below that temperature peak position and shape of basic reflections were maintained, even as the intensity of 004 reflection gradually decreases due to crystalline water loss (see Appendix Asupporting information II). Above 453 K, however, the hydrate gradually transforms to an orthorhombic phase. The tetragonal hydrate and orthorhombic phase coexist between 453 and 493 K. It seems likely such a reaction as represented by Eq. (3) takes place:

$$ZrW_{2.00-y}V_yO_{7.00-y/2}(OH)_{2.00}(H_2O)_{2.00}=ao\text{-}ZrW_{2.00-y}V_yO_{8.00-y/2}$$
$$+(1-a)ZrW_{2.00-y}V_yO_{7.00-y/2}(OH)_{2.00}(H_2O)_{2.00-z'}$$
$$+\delta'H_2O \quad (y=0.0.20) \tag{3}$$
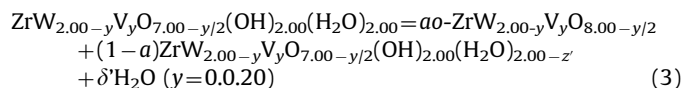
This indicates that the hydrates start losing compositional hydroxo-(O–H) groups while continuing losing crystalline water and begin transforming to orthorhombic phase (o-ZrW$_{2.00-y}$V$_y$O$_{8.00-y/2}$). Through quantitative FTIR measurement of ZrW$_{2.00-y}$V$_y$O$_{7.00-y/2}$(OH)$_{2.00}$(H$_2$O)$_{2.00-z'}$ at various degrees of dehydration (different $\delta'$ values in reaction (3)) and based on a linear relationship between ($A_{H_2O}/A_{OH}$) and ($C_{H_2O}/C_{OH}$), ($C_{H_2O}/C_{OH}$) can be
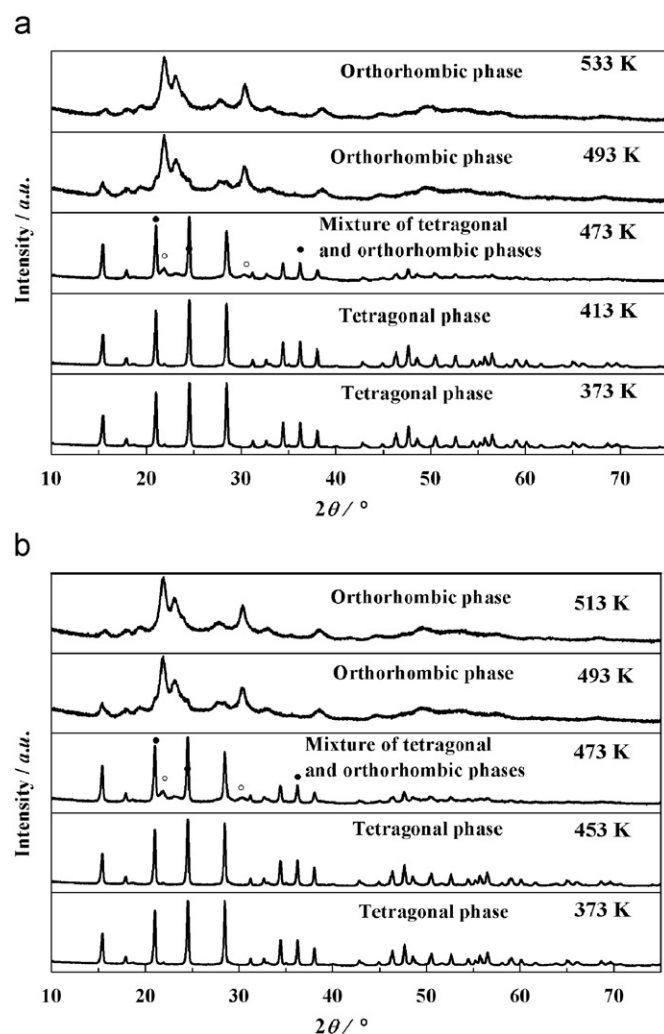
a



b



**Fig. 5.** Variable temperature XRD (○:orthorhombic phase; ●:tetragonal phase) of ZrW$_2$O$_7$(OH)$_2$(H$_2$O)$_2$ (a) and ZrW$_{1.80}$V$_{0.20}$O$_{6.90}$(OH)$_2$(H$_2$O)$_2$ (b).

indirectly measured. The crystalline water amount 2.00−$z'$ and the orthorhombic phase content $a$ were then calculated based on $C_{H_2O}/C_{OH}=2/(2-z')$ and $\delta'=3a+(1-a)z'$. The relationship between $a$ and (2.00−$z'$) is shown in Fig. 6.

Fig. 6 clearly reveals the existence of two steps in dehydration process. At the initial stage of dehydration ($\delta'<1.6$), crystalline water content (2.00−$z'$) gradually decreases but remains above 1. The amount of orthorhombic phase ($a$) is relatively small and this implies that most water loss is due to crystalline water. At the latter stage of dehydration ($\delta'>1.6$), the structure loses both remaining crystalline water and compositional hydroxo-(O–H) group and transforms to orthorhombic phase at the same time.

The dehydration process completes at about 500 K. XRD patterns of the complete dehydration product were indexed in the orthorhombic crystal system with $a$=5.56 (1) Å, $b$=7.24(1) Å, $c$=9.05 (1) Å for o-ZrW$_{2.00}$O$_{8.00}$ and $a$=5.66 (1) Å, $b$=7.20 (1) Å, $c$=9.08 (1) Å for o-ZrW$_{1.80}$V$_{0.20}$O$_{7.90}$ as shown in Fig. 7, which is similar to the reported LT-ZrMo$_2$O$_8$ with the lattice parameters $a$=5.879 Å, $b$=7.316 Å, $c$=9.139 Å [28].

Configuration of the substitution V in the orthorhombic phase ZrW$_{1.80}$V$_{0.20}$O$_{6.90}$(OH)$_{2.00}$(H$_2$O)$_{2.00}$ was studied by variable temperature Raman spectra from 373 to 573 K as shown in Fig. 8 .

The Raman spectrum changes little below 473 K. Above 473 K the Raman intensity at 963 cm$^{-1}$ gradually decreases and broadens with increasing temperature. Between 473 and 513 K, Raman
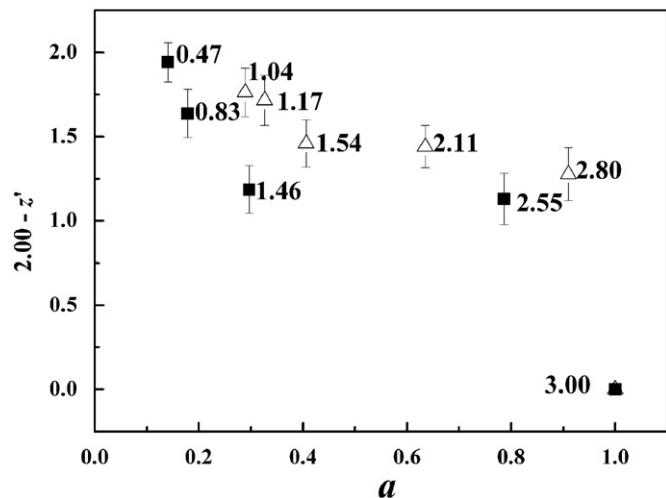
**Fig. 6.** Relationship between the crystalline water amount $2.00 - z'$ and the orthorhombic phase content $a$ above dehydroxyl temperature for $ZrW_{2.00-y}V_yO_{7.00-y/2}(OH)_{2.00}(H_2O)_{2.00}$ (■ : $y=0$; △ : $y=0.20$) ($\delta'$ values in Eq. (3) are labeled by the data points, error bars were represented in the figure).
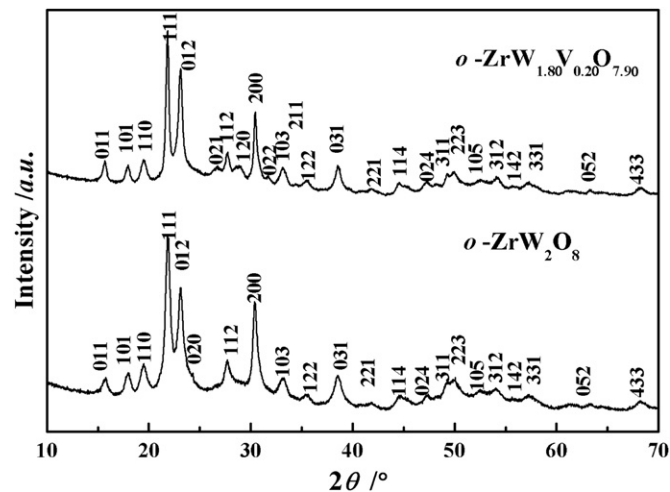


**Fig. 7.** Indexed X-ray diffraction patterns of $o$-$ZrW_2O_8$ and $o$-$ZrW_{1.80}V_{0.20}O_{7.90}$.
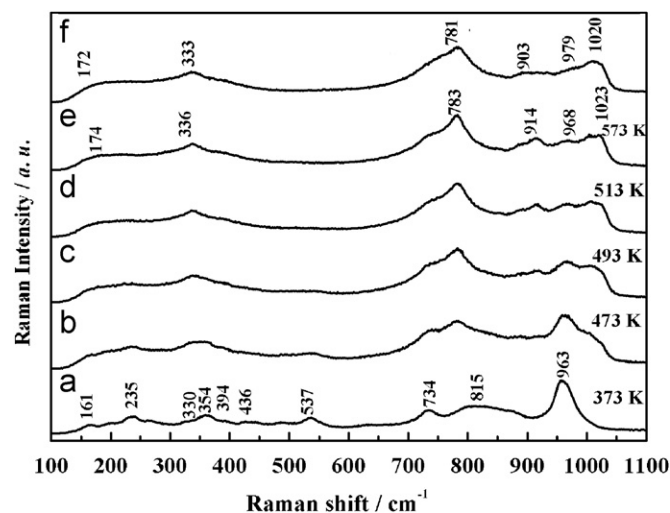


**Fig. 8.** Variable temperature Raman spectra of $ZrW_{1.80}V_{0.20}O_{6.90}(OH)_{2.00}(H_2O)_{2.00}$ (a: 373 K; b: 473 K; c : 493 K; d : 513 K; e : 573 K and f: $o$-$ZrW_{2.00}O_{8.00}$).

frequencies at 963, 814, 735, 535, and 354 cm$^{-1}$ due to W/VO$_6$ polyhedral vibration gradually submerge, while Raman bands at 1023, 914, 783, and 336 cm$^{-1}$ due to W/VO$_4$ polyhedral [29] emerge. At 513 K the phase transition completes and Raman peaks due to W/VO$_6$ polyhedral vibration disappear and only vibrations from W/VO$_4$ polyhedra are observed. The Raman spectra of dehydrated $o$-$ZrW_{2.00}O_{8.00}$ and $o$-$ZrW_{1.80}V_{0.20}O_{7.90}$ solid solutions are almost identical. The frequency shifts of bands associated with [W/V]O$_4$ polyhedral vibration are insignificant. These results are consistent with a structure model that vanadium atoms stoichiometrically occupy tungsten sites to produce a substitutional orthorhombic $ZrW_{1.80}V_{0.20}O_{7.90}$ solid solution.

By annealing $ZrW_{1.80}V_{0.20}O_{7.90}$ at 813 K in 2 h orthorhombic phase completely transforms to cubic-$ZrW_{1.80}V_{0.20}O_{7.90}$ ($c$-$ZrW_{1.80}V_{0.20}O_{7.90}$).

### 3.3. Properties of cubic $ZrW_{1.80}V_{0.20}O_{7.90}$

The XRD pattern of cubic $ZrW_{1.80}V_{0.20}O_{7.90}$ at 300 K was indexed based on the $\alpha$-$ZrW_2O_8$ structure (Space Group: $P2_13$) with superstructure reflection 310 indicating partial structure ordering (hereafter denoted as $\alpha$-$ZrW_{1.80}V_{0.20}O_{7.90}$).

The lattice parameter of $\alpha$-$ZrW_{1.80}V_{0.20}O_{7.90}$ at 284 K is 9.1303 (1) Å, which is smaller than that of $\alpha$-$ZrW_2O_8$ (9.1575 Å at room temperature) [1a]. It continuously decreases as temperature
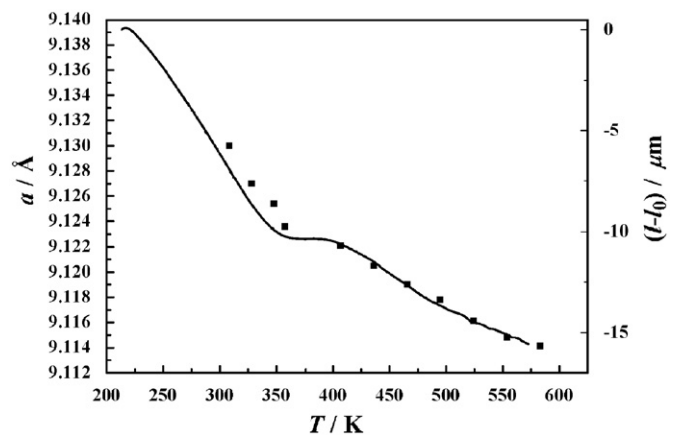


**Fig. 9.** Cell parameter $a$ and bulk ceramic dimension change ($l$–$l_0$) of $\alpha$-$ZrW_{1.80}V_{0.20}O_{7.90}$ with temperatures.
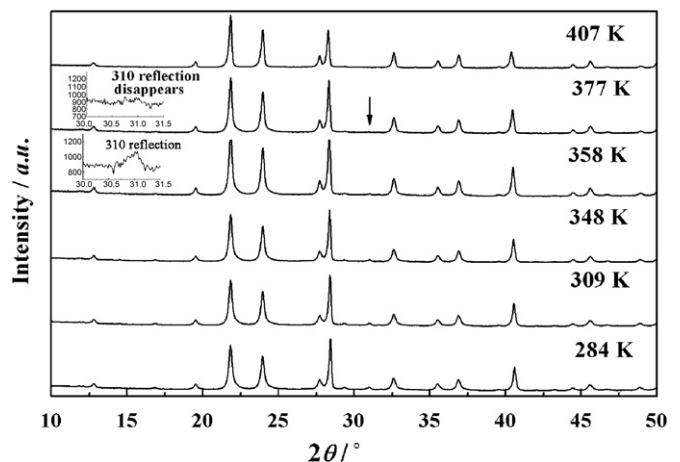


**Fig. 10.** X-ray diffraction patterns of $ZrW_{1.80}V_{0.20}O_{7.90}$ at different temperatures. The section arrow marked is expanded as inset (the peak at about 28.3° is from the internal standard KCl).

increases similar to the thermal contraction property of $c$-$ZrW_2O_8$ as shown in Fig. 9. Between 284 and 358 K, coefficient of thermal expansion [CTE: $(a-a_0)/a_0(T-T_0)$] is $-9.7 \times 10^{-6}$ K$^{-1}$ comparable to that of $\alpha$-$ZrW_2O_8$ ($-9.07 \times 10^{-6}$ K$^{-1}$ in 2–350 K temperature range) [30]; in the 400–575 K range, where is in its $\beta$-$ZrW_{1.80}V_{0.20}O_{7.90}$ form, CTE is $-1.6 \times 10^{-6}$ K$^{-1}$ and larger than that of $\alpha$-$ZrW_2O_8$ ($-6 \times 10^{-6}$ K$^{-1}$ in 423–693 K temperature range) [1a]. Dimension measurements on bulk ceramic sample, also displayed in Fig. 9, are consistent with cell parameter change.

The bulk ceramic dimension as a function of temperature further shows a continuous phase transition. From Fig. 10 of variable temperature XRD data, it is seen the inten sity of super-structure reflection 310 continuously decreases with increasing temperature until about 377 K which is lower than that of $ZrW_2O_8$ ($T_c = 448$ K) [30].

## 4. Conclusion

Based on chemical and structural similarities between $ZrV_2O_7$ and $ZrW_2O_8$, synthesis of a novel aliovalent W-site substituted cubic $ZrW_{1.80}V_{0.20}O_{7.90}$ was successfully achieved. As the precursor of $c$-$ZrW_{1.80}V_{0.20}O_{7.90}$ a tetragonal $ZrW_{1.80}V_{0.20}O_{6.90}(OH)_{2.00}$-$(H_2O)_{2.00}$ hydrate, is obtained through an ASH process. The XRD and Raman measurement support that vanadium atom remains in solid solution state during the dehydration and phase transition process. This fact is crucial to the formation of $c$-$ZrW_{1.80}V_{0.20}O_{7.90}$ through ASH–TDP route. The synthesis mechanism of $c$-$ZrW_{1.80}V_{0.20}O_{7.90}$ from $ZrW_{1.80}V_{0.20}O_{6.90}(OH)_{2.00}(H_2O)_{2.00}$ is similar to the formation of $\gamma$-$ZrMo_2O_8$ from $ZrMo_2O_7(OH)_2(H_2O)_2$ [28]. The details of $ZrW_{1.80}V_{0.20}O_{6.90}(OH)_{2.00}(H_2O)_{2.00}$ dehydration process is revealed by variable temperature XRD and quantitative FTIR to be a two step process where crystalline water first takes off partially at lower temperature and the tetragonal hydrate becomes unsaturated; above certain temperature, compositional hydroxo-(O–H) group as well as crystal water remove simultaneously producing a metastable orthorhombic $ZrW_{1.80}V_{0.20}O_{7.90}$ phase as the important intermediate product.

Measurement of the cell parameter change with temperature indicates that the cubic $ZrW_{1.80}V_{0.20}O_{7.90}$ retains thermal contraction property of the cubic $ZrW_2O_8$. The average linear thermal expansion coefficients of $\alpha$- and $\beta$-$ZrW_{1.80}V_{0.20}O_{7.90}$ are $-9.7 \times 10^{-6}$ K$^{-1}$ (284–358 K) and $-1.6 \times 10^{-6}$ K$^{-1}$ (400–575 K), respectively.

## Acknowledgment

## Appendix A. Supplementary material

Supplementary data associated with this article can be found in the online version at doi:10.1016/j.jssc.2011.03.021.

## References

[1] (a) J.S.O. Evans, T.A. Mary, T. Vogt, M.A. Subramanian, A.W. Sleight, Chem. Mater. 8 (1996) 2809–2823;
(b) T.A. Mary, J.S.O. Evans, T. Vogt, A.W. Sleight, Science 272 (1996) 90–92;
(c) G. Ernst, C. Broholm, G.R. Kowach, A.P. Ramirez, Nature 396 (1998) 147–149;
(d) J.S.O. Evans, Z. Hu, J.D. Jorgensen, D.N. Argyriou, S. Short, A.W. Sleight, Science 275 (1997) 61–65;
(e) A.P. Ramirez, G.R. Kowach, Phys. Rev. Lett. 80 (1998) 4903–4906;
(f) T.R. Ravindran, A.K. Arora, T.A. Mary, Phys. Rev. Lett. 84 (2000) 3879–3882;
(g) D. Cao, F. Bridges, G.R. Kowach, A.P. Ramirez, Phys. Rev. Lett. 89 (2002) 215902/1–215902/4;
(h) J.N. Hancock, C. Turpen, Z. Schlesinger, Phys. Rev. Let. 93 (2004) 225501/1–225501/4;
(i) R. Mittal, S.L. Chaplot, N. Choudhury, Prog. Mater. Sci. 51 (2006) 211–286;
(j) C.A. Figueirêdo, C.A. Perottoni, Phys. Rev. B 75 (2007) 184110/1.
[2] (a) Y. Yamamura, K. Masago, M. Kato, T. Tsuji, J. Phys. Chem. B 111 (2007) 10118;
(b) Y. Yamamura, N. Nakajima, T. Tsuji, A. Kojima, Y. Kuroiwa, A. Sawada, S. Aoyagi, H. Kasatani, Phys. Rev. B 70 (2004) 104107/1–104107/6.
[3] (a) H.H. Li, H.T. Xia, X.P. Jing, X.H. Zhao, Solid State Commun. 142 (2007) 434–436;
(b) H.H. Li, H.T. Xia, X.P. Jing, X.H. Zhao, Solid State Sci. 10 (2008) 1037–1041.
[4] C. Lind, D.G. VanDerveer, A.P. Wilkinson, J.H. Chen, M.T. Vaughan, D.J. Weidner, Chem. Mater. 13 (2001) 487–490.
[5] (a) L. Huang, Q.G. Xiao, H. Ma, G.B. Li, F.H. Liao, Ch.M. Qi, X.H. Zhao, J. Eur., Inorg. Chem. 22 (2005) 4521–4526;
(b) Y.F. Shi, J.S. Han, X. Chen, H. Ma, X.X. Li, X.J. Yang, X.H. Zhao, J. Solid State Chem. 182 (2009) 2030–2035.
[6] H.H. Li, J.S. Han, H. Ma, L. Huang, X.H. Zhao, J. Solid State Chem. 180 (2007) 852–857.
[7] K. DeBuysser, I. VanDriessche, B. VandePutte, P. Vanhee, J. Schaubroeck, S. Hoste, Inorg. Chem. 47 (2008) 736–741.
[8] C. DeMeyer, F. Bouree, J.S.O. Evans, K. DeBuysser, E. Bruneel, I. VanDriessche, S. Hostea, J. Mater. Chem. 14 (2004) 2988–2994.
[9] Y. Yamamura, N. Nakajima, T. Tsuji, Phys. Rev. B 64 (2001) 184109/1–184109/5.
[10] N. Nakajima, Y. Yamamura, T. Tsuji, Solid State Commun. 128 (2003) 193–196.
[11] (a) C. Closmann, A.W. Sleight, J.C. Haygarth, J. Solid State Chem. 139 (1998) 424–426;
(b) S. Allen, J.S.O. Evans, J. Mater. Chem. 14 (2004) 151–156;
(c) R.Q. Zhao, X.J. Yang, H.L. Wang, J.S. Han, H. Ma, X.H. Zhao, J. Solid State Chem. 180 (2007) 3160–3165;
(d) J.S.O. Evans, P.A. Hanson, R.M. Ibberson, N. Duan, U. Kamesward, A.W. Sleight, J. Am. Chem. Soc. 122 (2000) 8694–8699.
[12] V. Korthuis, N. Khosrovani, A.W. Sleight, N. Roberts, R. Dupree, W.W. Warren, Chem. Mater. 7 (1995) 412–417.
[13] A.K.A. Pryde, K.D. Hammonds, M.T. Dove, V. Heine, J.D. Gale, M.C. Warren, J. Phys.: Condens. Matter 8 (1996) 10973–10982.
[14] N. Khosrovani, A.W. Sleight, J. Solid State Chem. 132 (1997) 355–360.
[15] X. Chen, J.Z. Tao, H. Ma, X.H. Zhao, Acta Cryst. C. 65 (2009) 74–76.
[16] X.B. Deng, X.H. Zhao, J.S. Han, Chin. J. Inorg. Chem. 21 (2005) 1357–1360.
[17] C. Dong, J. Appl. Cryst. 32 (1999) 838.
[18] T.J.B. Holland, S.A.T. Redfern, Miner. Magaz. 61 (1997) 65–77.
[19] P.D. Pathak, N.G. Vasavada, Acta Cryst. A 26 (1970) 655–658.
[20] A.C. Larson, R.B. Von Dreele, General Structure Analysis System (GSAS), Los Alamos National Laboratory Report LAUR (2000) 86–748.
[21] A. Clearfield, R.H. Blessing, J. Inorg. Nucl. Chem. 34 (1972) 2643–2652.
[22] T.A. Instruments-Waters LLC (U.S. Patent No. 6, 007, 240).
[23] (a) A.F. Gualtieri, J. Appl. Cryst. 33 (2000) 267–278;
(b) A.G. Torre, S. Bruque, M.A. Aranda, J. Appl. Cryst. 34 (2001) 196–202.
[24] A. Clearfield, R.H. Blessing, J. Inorg. Nucl. Chem. 36 (1974) 1174–1176.
[25] F.D. Hardcastle, I.E. Wachs, J. Raman Spectrosc. 26 (1995) 397–405.
[26] Z.C. Ling, H.R. Xia, S.Q. Sun, D.G. Ran, F.Q. Liu, P. Zhao, C.Y. Gao, J.X. Zhang, J.Y. Wang, J. Appl. Phys. 100 (2006) 043522/1–043522/6.
[27] Bianca Montanari, Anne J. Barbosa, Sidney J.L. Ribeiro, Younes Messaddeq, Gael Poirier, Maximo S. Li, Appl. Surf. Sci. 254 (2008) 5552–5556.
[28] A. Simon, R.W. Nicholas, K.B.G. Richard, J.S.O. Evans, Chem. Mater. 15 (2003) 3406–3410.
[29] E.J. Liang, Y. Liang, Y. Zhao, J. Liu, Y. Jiang, J. Phys. Chem. A 112 (2008) 12582–12587.
[30] J.S.O. Evans, W.I.E. David, A.W. Sleight, Acta Cryst. B55 (1999) 333–340.